Editors' Suggestion

Giant Piezoelectric Effects of Topological Structures in Stretched Ferroelectric Membranes

Yihao Hu,[1] Jiyuan Yang,[1] and Shi Liu[1,2,*]

[1]Key Laboratory for Quantum Materials of Zhejiang Province, Department of Physics, School of Science, Westlake University, Hangzhou, Zhejiang 310024, China

[2]Institute of Natural Sciences, Westlake Institute for Advanced Study, Hangzhou, Zhejiang 310024, China

(Received 2 February 2024; accepted 18 June 2024; published 26 July 2024)

Freestanding ferroelectric oxide membranes emerge as a promising platform for exploring the interplay between topological polar ordering and dipolar interactions that are continuously tunable by strain. Our investigations combining density functional theory (DFT) and deep-learning-assisted molecular dynamics simulations demonstrate that DFT-predicted strain-driven morphotropic phase boundary involving monoclinic phases manifest as diverse domain structures at room temperatures, featuring continuous distributions of dipole orientations and mobile domain walls. Detailed analysis of dynamic structures reveals that the enhanced piezoelectric response observed in stretched $PbTiO_3$ membranes results from small-angle rotations of dipoles at domain walls, distinct from conventional polarization rotation mechanism and adaptive phase theory inferred from static structures. We identify a ferroelectric topological structure, termed "dipole spiral," which exhibits a giant intrinsic piezoelectric response (> 320 pC/N). This helical structure, possessing a rotational zero-energy mode, unlocks new possibilities for exploring chiral phonon dynamics and dipolar Dzyaloshinskii-Moriya-like interactions.

DOI: 10.1103/PhysRevLett.133.046802

Strain engineering of ferroelectric oxides through thin film epitaxy has greatly advanced the understanding of ferroelectric physics and led to the realization of novel topological polar structures and functionalities [1–3]. By exploiting the lattice mismatch between ferroelectric oxides and their substrates, the interactions among spin, charge, orbital, lattice, and domain degrees of freedom can be deterministically controlled [4]. Nevertheless, the effectiveness of epitaxial strain is generally limited to ≈2%. Beyond this threshold, defects and dislocations tend to form at the ferroelectric-substrate interface, leading to strain relaxation [5]. The number of strain states for a ferroelectric oxide is further restricted by the availability of high-quality substrates. Recent advancements in synthesizing single-crystal, freestanding oxide membranes have opened new avenues [6–8], enabling strain states up to an unprecedented level (≈8%) [9,10] and integration with silicon-based technologies [11,12]. Moreover, the freestanding membrane, adaptable to continuously variable isotropic and anisotropic strains [8], allows for in-depth investigations into the intricate interplay between topological polar ordering and dipole correlations. A general approach to predicting the strain phase diagram under experimental conditions will facilitate the discovery of novel emergent phenomena in ferroelectric membranes. The challenge is to bridge the gap between zero-Kelvin, first-principles-based, unit-cell-level calculations, and measurable macroscopic properties, which are often significantly influenced by mesoscopic domain structures.

Pertsev *et al.* pioneered the mapping of ferroelectric perovskite structures against temperature and misfit strain using Landau-Devonshire theory based on empirical thermodynamic potentials [13]. Dieguez *et al.* subsequently demonstrated that predictions from this method are sensitive to parameters fitted to experimental data, highlighting the importance of an *ab initio* approach [14]. Although first-principles density functional theory (DFT) is commonly used to predict phase diagrams [15,16], the single-domain approximation introduced to reduce computational costs neglects the impacts of domain structures. In contrast, phase-field methods, effective in predicting three-dimensional (3D) domain structures, rely heavily on empirical parameters and lack atomic-level details. Here, we employ deep potential molecular dynamics (DPMD) [17] simulations to construct phase diagrams at finite temperatures, advancing beyond the single-domain assumption.

Taking $PbTiO_3$ membranes, for example, we show that while DFT calculations indicate a tensile-strain-driven morphotropic phase boundary (MPB) with competing phases [18], this feature becomes absent in thermally active environments. Instead, the flat potential energy landscape results in diverse domain structures with flexible dipoles and mobile domain walls. DPMD simulations reveal that the dynamic structure of the c/a two-domain state exhibits a broad and continuous distribution of dipole orientations. The collective and coordinated small-angle rotations of dipoles at domain walls underlie the enhanced piezoelectric

*Contact author: liushi@westlake.edu.cn

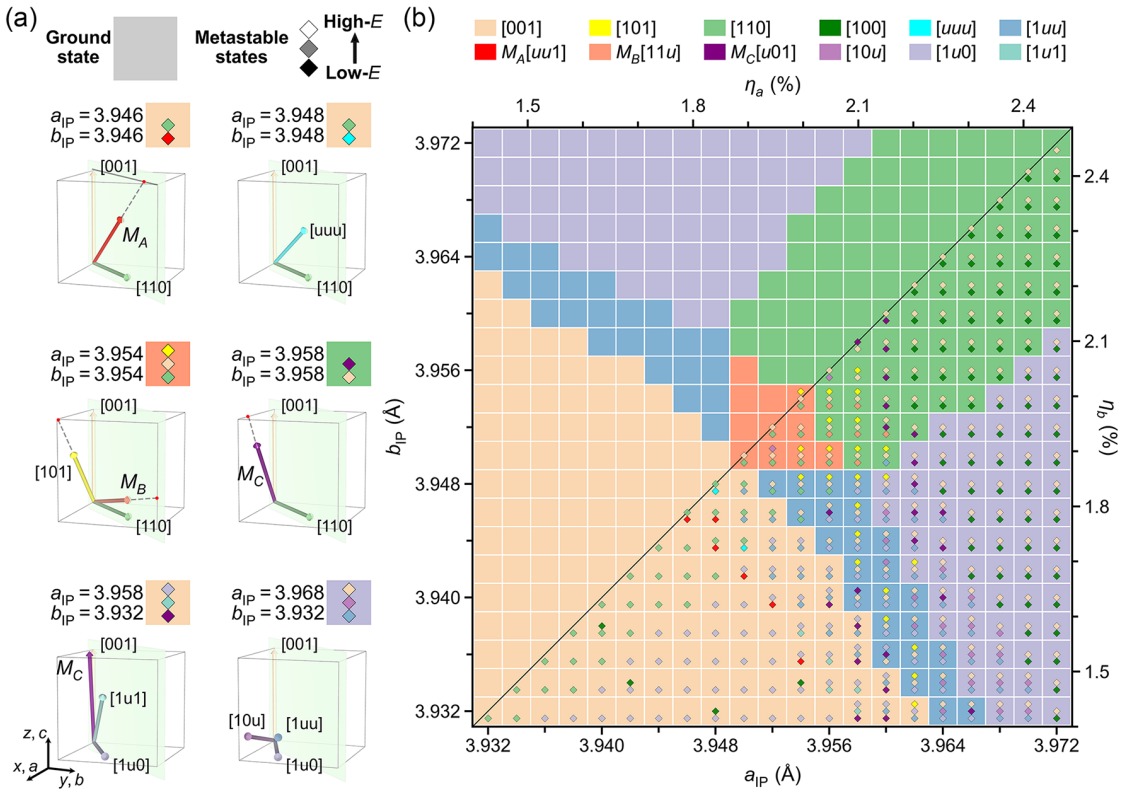

FIG. 1. DFT strain multiphase diagram for $PbTiO_3$ membranes. (a) Unique polar states stabilized by tensile strains. A plaquette in the phase diagram encodes all possible phases that a five-atom unit cell can sustain under a specific strain condition. The square's background color corresponds to the ground state, while other metastable phases are indicated by markers arranged vertically by their energies (E). (b) Phase diagram illustrating the competitions among phases with comparable energies. Considering the exchange symmetry between in-plane a and b axes, the phase compositions are explicitly depicted only within the bottom right triangular region. The strain η is computed relative to the DFT ground-state value ($a_0 = b_0 = 3.877$ Å).

strain coefficient (d_{33}) observed experimentally in stretched $PbTiO_3$ membranes [19], distinct from conventional polarization rotation mechanism [20,21] and adaptive phase theory [22,23]. Interestingly, further stretching the membrane could activate spontaneous and stochastic oscillations of 90° domain walls, leading to an even higher d_{33} value of ≈250 pC/N, 3 times that of a single domain (≈80 pC/N). We further discover a ferroelectric topological structure, the dipole spiral, characterized by canted dipoles that progressively rotate around the out-of-plane direction. This helical dipolar structure supports a giant piezoelectric response (> 320 pC/N) through small-angle dipole rotations.

We start by constructing the strain phase diagram for $PbTiO_3$ across a wide range of tensile strains, based on high-throughput DFT calculations. These calculations serve as a mean-field-like analysis for energy variation with respect to polarization (P) orientation. All first-principles calculations are performed with the projector augmented-wave (PAW) method [24,25], using the Vienna *ab initio* simulation package (VASP) [26,27]. The exchange-correlation functional is treated within the generalized gradient approximation of Perdew-Burke-Ernzerhof revised for solids (PBEsol) type [28]. For a given strain state, the in-plane lattice parameters (a_{IP} and b_{IP}) of a five-atom unit cell are fixed, while the atomic coordinates and out-of-plane lattice constant are fully optimized. This setup closely resembles the application of orthogonal strains to freestanding membranes, which is a common scenario in experimental settings [8,9,19]. To access competing polar states, multiple initial configurations with polarization pointing in different directions are used. A kinetic energy cutoff of 800 eV, a k-point spacing of 0.3 $Å^{-1}$ for the Brillouin zone integration, and a force convergence threshold of 0.001 eV/Å are used to converge the energy and atomic forces.

We introduce a "multiphase" diagram to illustrate the competitions among phases with comparable energies (within 6 meV/atom). Twelve unique polar states [see Fig. 1(a)] are identified, each categorized by the polarization direction while considering the exchange symmetry between in-plane a and b axes. For strains close to equal-biaxial conditions ($a_{IP} = b_{IP}$), we observe some well-known phases: a tetragonal (T) phase with its polarization along the pseudocubic [001] axis; orthorhombic (O) [110] and [101] phases with polarization along the face diagonal directions; and a rhombohedral (R, denoted as [111]) phase with nearly equal magnitudes of P_x, P_y, and P_z. There are

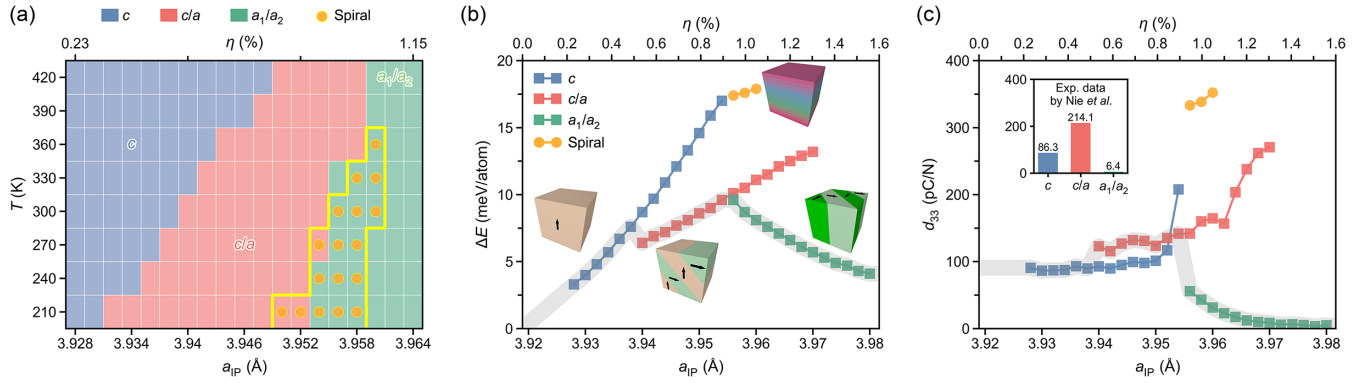

FIG. 2. Thermodynamic stability and piezoelectric response of domain structures. (a) MD strain-temperature domain stability diagram. The yellow-colored boundary highlights the strain states supporting dipole spirals. The strain η is computed in reference to the MD ground-state value at 300 K ($a_0 = b_0 = 3.919$ Å). (b) Relative thermodynamic stability and (c) piezoelectric coefficients of different domain structures with respect to isotropic in-plane strains at 300 K. The thick shaded line traces the most stable domain structure. The inset reports experimental d_{33} values of $PbTiO_3$ membranes [19].

also three monoclinic phases introduced by Vanderbilt and Cohen [29]: M_A with $P_x \approx P_y < P_z$ (denoted as $[uu1]$ with $u < 1$), serving as a bridge between the [001] and [111] phases; M_B with $P_x \approx P_y > P_z$ (denoted as $[11u]$), which connects the [110] and [111] phases; and M_C with a space group of Pm (denoted as $[u01]$), intermediate between the [001] and [101] phases. A strongly anisotropic biaxial strain induce four additional phases: two distorted R phases, $[1uu]$ with $P_x > P_y \approx P_z$ and $[1u1]$ with $P_x \approx P_z > P_y$, and two distorted O phases, $[1u0]$ and $[10u]$. Finally, under a sufficiently large tensile strain along the a axis, the [100] state becomes competitive. It is evident from Fig. 1(b) that a variety of strain conditions can stabilize multiple phases. For example, at $a_{IP} = b_{IP} = 3.946$ Å, the energies of [001], M_A, and [110] phases are within 1 meV/atom.

The multiphase diagram suggests that a tensile in-plane strain leads to a flat potential energy landscape with respect to polarization rotation in $PbTiO_3$, a hallmark of MPB [30]. The emergence of phase competitions involving various M phases supports an M-phase-mediated polarization rotation mechanism [31,32]. The question is whether this MPB-like feature persists at finite temperatures. To address this, we perform large-scale DPMD simulations to investigate the polar ordering at finite temperatures. For simplicity, we focus on isotropic in-plane strains ($a_{IP} = b_{IP}$). The DP model can reproduce various properties of $PbTiO_3$, including phonon spectra of tetragonal and cubic phases, the temperature-driven phase transition, and topological textures such as polar vortex lattice in $PbTiO_3/SrTiO_3$ superlattices [33]. We have developed an online notebook [34] on Github to share the training database, force field model, training metadata, and essential input and output files. Further details about MD simulations using LAMMPS [35] can be found in Supplemental Material [36].

The strain-temperature domain stability diagram is presented in Fig. 2(a), revealing three well-known domain structures and a novel, metastable topological structure that resembles a spin spiral [39,40]. The three recognized domain morphologies are a single c-domain state comprised solely of [001] domains; a c/a two-domain state with [001] and [100] (or [010]) domains; and an a_1/a_2 two-domain state with [100] and [010] domains. Predicted without empirical parameters, the strain-driven evolution of these domain structures, $c \rightarrow c/a \rightarrow a_1/a_2$, agrees well with results from phase-field simulations [41,42]. The topological structure, which we name "dipole spiral," features canted dipoles that progressively rotate around the [001] direction (see detailed discussions below). Figure 2(b) plots the energies of domain structures at 300 K against a_{IP}. For certain strains (η, computed relative to the ground-state in-plane lattice constant of the c-domain $PbTiO_3$ at 300 K), multiple domain morphologies can coexist. For example, in the range of $0.94\% < \eta < 1.05\%$, a_1/a_2, c/a, and the dipole spiral are all stable in MD simulations. The dipole spiral, albeit energetically higher than the lowest-energy state, demonstrates significant robustness across a broad temperature and strain range [Fig. 2(a)]. It is noted that we observe a discontinuous evolution from a c-domain state to a dipole spiral at a critical strain of $a_{IP} \approx 3.954$ Å (see Fig. S12 [36]). These findings convey that MPB-like phase competitions, predicted by zero-Kelvin DFT calculations, actually manifest as complex domain structures at finite temperatures, prompting an essential inquiry: can the domain structure enhance the piezoelectric response in the absence of MPB?

Using finite-field MD simulations, we quantify d_{33} of stretched membranes via the direct piezoelectric effect, $[\partial\eta_3/\partial\mathcal{E}_3]|_{\sigma_3=0}$, where η_3 is the strain change along the z axis due to an out-of-plane electric field ($\mathcal{E}_3$). Figure 2(c) shows that the c/a domain structure yields larger d_{33} values than the single c domain under the same strain conditions ($3.94 < a_{IP} < 3.955$ Å), indicating 90° domain walls

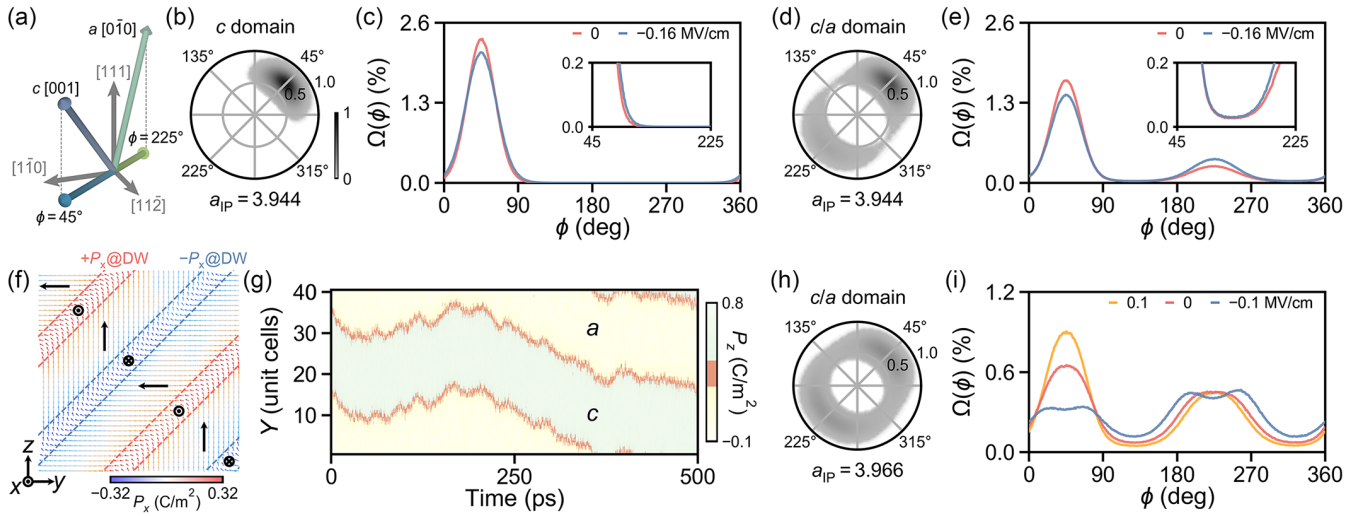

FIG. 3. Enhanced piezoelectricity in stretched $PbTiO_3$ membranes with c/a two-domain states. (a) Schematic illustration of a $[0\bar{1}0]$ dipole in the a domain and a [001] dipole in the c domain projected onto the {111} plane. Dipole orientation distributions in (b)–(c) single-c domain, and (d)–(e), c/a two-domain states under the same strain condition ($a_{IP} = 3.944$ Å). The distributions are plotted in polar coordinates viewed along [111] in (b) and (d). The distributions of azimuthal angles (ϕ) in the {111} plane and their changes to an out-of-plane field ($\mathcal{E}_3$) are presented in (c) and (e), with insets providing enlarged views. (f)–(i) c/a domain structures in strongly stretched membranes ($a_{IP} = 3.966$ Å). Arrows representing local dipoles are colored based on P_x components in (f). The 90° domain walls separating $-P_y$ and $+P_z$ domains exhibit substantial P_x components and adopt antiferroelectric coupling between neighboring walls. (g) Spontaneous stochastic oscillating 90° domain walls in the absence of external electric fields. (h)–(i) Dipole orientation distributions in strongly stretched c/a domain structures.

enhance the piezoelectric response. For higher tensile strains ($a_{IP} > 3.955$ Å), which favor the a_1/a_2 state, d_{33} diminishes rapidly due to minimal out-of-plane polarization. The concave characteristic of the d_{33} versus a_{IP} curve, highlighted by the thick shaded line in Fig. 2(c), agrees quantitatively with the trend observed in experiments with freestanding $PbTiO_3$ membranes [19]. Notably, the d_{33} value of the c/a state experiences a jump when a_{IP} is beyond a critical value of 3.962 Å, surpassing 250 pC/N and significantly exceeding the bulk value of ≈80 pC/N.

To comprehend the strain-dependent d_{33} of the c/a domain structure, we calculate the distributions of dipole (unit-cell polarization) orientations in both single c-domain and c/a two-domain states at the same strain of $a_{IP} = 3.944$ Å, using configurations sampled from equilibrium MD trajectories of at least 20 ps. This approach provides a statistical perspective on the dynamic structure. The dipole orientation is gauged by its azimuthal angle (ϕ) in the [111] plane [Fig. 3(a)] to better distinguish c ([001]) and a ($[0\bar{1}0]$) domains. As shown in Figs. 3(b) and 3(c), the single c domain features a ϕ distribution peaking at 45°. In contrast, the dynamic structure of the c/a state [Figs. 3(d) and 3(e)] has a ϕ distribution ranging continuously from 0° and 360°, with broadened peaks at 45° and 225°, corresponding to [001] and $[0\bar{1}0]$ dipoles, respectively. Dipoles with angle values deviating from the two main peaks are mainly near 90° domain walls, serving as continuously varying intermediate states bridging a and c domains. This marked difference in dynamic structure between the single c-domain and c/a two-domain states is also evident in polar coordinates [Figs. 3(b) and 3(d)]. In response to $\mathcal{E}_3$, dipoles in the single c domain rotate away from the [001] direction, reducing the peak height at 45° [Fig. 3(c)]. In comparison, the same $\mathcal{E}_3$ induces more pronounced changes to the distribution in the c/a state [Fig. 3(e)], indicating that the enhanced d_{33} results from the collective and coordinated small-angle rotations of dipoles at domain walls, analogous to "coordinated gear dynamics," rather than the conventional understanding of 90° polarization rotation between domains [43,44]. Additionally, the dipole orientation distribution associated with the dynamic structure does not show well-defined intermediate phases.

The rapid rise in d_{33} for the c/a domain structure beyond a critical tensile strain coincides with the emergence of substantial polarization components within domain walls [45], as well as a sharper increase in the domain wall thickness (see Fig. S15 [36]). As illustrated in Fig. 3(f), domain walls separating $-P_y$ and P_z domains exhibit $\pm P_x$ components, while adopting anti-parallel coupling between adjacent walls. Importantly, MD simulations reveal stochastic oscillations of these walls even without external driving forces [Fig. 3(g)], suggesting minimal barriers for small-angle dipole rotations near domain walls. This is consistent with the diffuse distribution of dipole orientations in polar coordinates [Fig. 3(h)] and the high susceptibility to $\mathcal{E}_3$ [Fig. 3(i)]. The mobile domain walls are

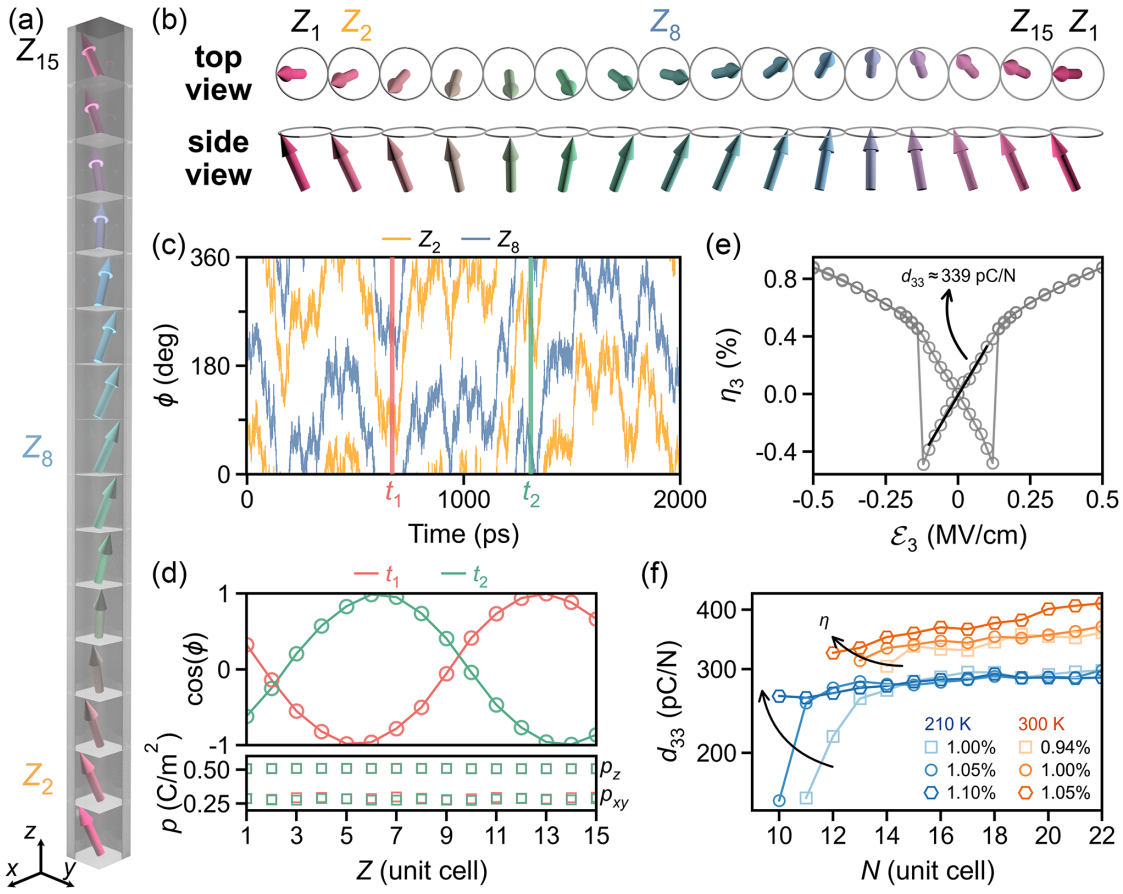

FIG. 4. Helical dipole spiral in stretched $PbTiO_3$ membranes at 300 K. (a)–(b) Schematic illustrations of dipole ordering in the spiral. (c) Evolution of instantaneous in-plane azimuth angles (ϕ) of dipoles in two different xy layers, Z_2 and Z_8, as labeled in (a). (d) Layer-resolved cos(ϕ) and polarization profiles of instantaneous configurations at t_1 and t_2 in (c). (e) Strain-electric field (η_3-$\mathcal{E}_3$) hysteresis loops for dipole spirals. (f) d_{33} as a function of N at varying strains and temperatures. The y axis is in log scale for clarity.

responsible for the giant d_{33} of > 250 pC/N. We note that the walls with P_x components can be switched by an electric field applied along the x axis, though the antiparallel coupling between adjacent walls is favored thermodynamically (see Supplemental Material [36], Sec. V.E).

We now focus on the helical dipole spiral, which supports an even larger piezoelectric response [$d_{33} > 320$ pC/N, see Fig. 2(c)]. The noncollinear ordering of dipoles, obtained by averaging configurations over a 100-ps MD trajectory at 300 K for a $15 \times 15 \times 15$ supercell, is depicted in Figs. 4(a) and 4(b). The spiral, with a propagation vector aligned along [001] and a wavelength of ≈15 unit cells, is robust as confirmed by MD simulations using various supercell sizes (Fig. S4 [36]). Specifically, the dipoles, tilted by ≈27° from the z axis [Fig. 4(a)], exhibit in-plane components that align collinearly but rotate 24° relative to the preceding layer [Fig. 4(b), top view]; the out-of-plane components remain largely unchanged [Fig. 4(b), side view].

We find that the dynamic structure of the dipole spiral is quite vibrant in two aspects. Figure 4(c) tracks the evolution of the instantaneous in-plane azimuth angles (ϕ) of dipoles in two different xy layers (denoted as Z_2 and Z_8, respectively), 6 unit cells apart along the [001] direction. The ϕ value for each individual layer fluctuates stochastically due to thermal activation, but the angle difference consistently remains around 144°, matching well with the expected 24° rotational difference per layer. Layer-resolved cos(ϕ) and polarization profiles of instantaneous configurations at two different time points (t_1 and t_2, separated by 640 ps) are plotted in Fig. 4(d), revealing the maintained helical configuration with shifted cos(ϕ) profiles and unchanged polarization magnitudes. These results indicate that the dipoles rotate collectively, coherently, and stochastically around the [001] direction and their collective response to external stimuli, achieved via small-angle rotations, is responsible for the giant piezoelectric effect. The simulated η_3-$\mathcal{E}_3$ hysteresis loop, shown in Fig. 4(e), further confirms the switchability of the dipole spiral (see MD snapshots in Fig. S6 [36]) as well as the reversible electromechanical coupling. This is distinct from the helical texture of electric dipoles in $BiCu_{0.1}Mn_{6.9}O_{12}$, which exhibits almost no out-of-plane polarization (< 20 μC/m^2) due to its improper nature [46].

We further investigate the effects of strain on the wavelength (measured in N unit cells) of dipole spirals and the

magnitude of d_{33} at two different temperatures, 210 and 300 K (see MD versus experimental temperatures in Fig. S13 [36]). As shown in Fig. 4(f), at 210 K and a tensile strain of 1%, the dipole spiral has a minimum wavelength limit: spirals with $N < 11$ will spontaneously transform into other domain structures in MD simulations, due to the increased gradient energy when N becomes small. Interestingly, dipole spirals with N up to 22 are all stable, showing no spontaneous transformation during the equilibrium process. This stability aligns with predictions from a Landau-Ginzburg-Devonshire (LGD) model developed for the dipole spiral (see Supplemental Material [36], Sec. IV), which reveals a slow increase in free energy as N increases. A larger tensile strain, such as 1.05% and 1.10%, reduces the minimum stable wavelength to $N = 10$. Overall, the strain has a weak impact on the magnitude of d_{33}, which stabilizes at ≈ 255 pC/N at 210 K. Increasing the temperature to 300 K pushes the minimum stable wavelength to larger values. For example, at a tensile state of 1%, we can only obtain dipole spirals with $N \geq 13$. The magnitude of d_{33} becomes more sensitive to both strain and N at 300 K, potentially achieving values greater than 400 pC/N. These results reveal a complex interplay between temperature, strain, wavelength, and piezoelectric response, highlighting the susceptible nature of dipole spirals.

Finally, we propose a feasible experimental approach to realize the dipole spiral. Our MD simulations of free-standing membranes of $PbTiO_3$, conducted with three-dimensional periodic boundary conditions, indicate that eliminating the depolarization field could facilitate the emergence of a dipole spiral. We design all-ferroelectric superlattices composed of alternating layers of $PbTiO_3$ and $Pb_{0.5}Sr_{0.5}TiO_3$ and find that this layered heterostructure supports arrays of dipole spirals in $Pb_{0.5}Sr_{0.5}TiO_3$ layers, each linking a pair of polar vortices within $PbTiO_3$ layers (see Fig. S16 [36]).

In summary, our findings demonstrate that dynamic structure dictates functional properties. For the extensively studied c/a two-domain state in $PbTiO_3$, we suggest that the enhanced piezoelectric effect arises from the collective, small-angle dipole rotations near domain walls. A dipole spiral in tensile-strained $PbTiO_3$ membranes is discovered, representing a new state of polar ordering with strongly correlated dipoles that can rotate freely without energy cost, indicative of a zero-energy mode. This topological polar structure offers an avenue for enhancing electromechanical coupling and exploring phenomena such as chiral phonon dynamics [47] and noncollinear ferroelectricity [48].

Acknowledgments—Y. H., J. Y., and S. L. acknowledge the supports from Natural Science Foundation of Zhejiang Province (2022XHSJJ006) and Westlake Education Foundation. We acknowledge useful discussions with Prof. Hongjian Zhao. The computational resource is provided by Westlake HPC Center.

[1] Y. Tang, Y. Zhu, X. Ma, A. Y. Borisevich, A. N. Morozovska, E. A. Eliseev, W. Wang, Y. Wang, Y. Xu, Z. Zhang *et al.*, Observation of a periodic array of flux-closure quadrants in strained ferroelectric $PbTiO_3$ films, Science **348**, 547 (2015).

[2] A. K. Yadav, Observation of polar vortices in oxide superlattices, Nature (London) **530**, 198 (2016).

[3] S. Das, Observation of room-temperature polar skyrmions, Nature (London) **568**, 368 (2019).

[4] R. Ramesh and D. G. Schlom, Creating emergent phenomena in oxide superlattices, Nat. Rev. Mater. **4**, 257 (2019).

[5] A. Fernandez, M. Acharya, H.-G. Lee, J. Schimpf, Y. Jiang, D. Lou, Z. Tian, and L. W. Martin, Thinfilm ferroelectrics, Adv. Mater. **34** (2022).

[6] D. Lu, D. J. Baek, S. S. Hong, L. F. Kourkoutis, Y. Hikita, and H. Y. Hwang, Synthesis of freestanding single-crystal perovskite films and heterostructures by etching of sacrificial water-soluble layers, Nat. Mater. **15**, 1255 (2016).

[7] G. Dong *et al.*, Super-elastic ferroelectric single-crystal membrane with continuous electric dipole rotation, Science **366**, 475 (2019).

[8] R. Xu, J. Huang, E. S. Barnard, S. S. Hong, P. Singh, E. K. Wong, T. Jansen, V. Harbola, J. Xiao, B. Y. Wang, S. Crossley, D. Lu, S. Liu, and H. Y. Hwang, Strain-induced room-temperature ferroelectricity in $SrTiO_3$ membranes, Nat. Commun. **11**, 3141 (2020).

[9] S. S. Hong, M. Gu, M. Verma, V. Harbola, B. Y. Wang, D. Lu, A. Vailionis, Y. Hikita, R. Pentcheva, J. M. Rondinelli, and H. Y. Hwang, Extreme tensile strain states in $La_{0.7}Ca_{0.3}MnO_3$ membranes, Science **368**, 71 (2020).

[10] S. Cai, Y. Lun, D. Ji, P. Lv, L. Han, C. Guo, Y. Zang, S. Gao, Y. Wei, M. Gu, C. Zhang, Z. Gu, X. Wang, C. Addiego, D. Fang, Y. Nie, J. Hong, P. Wang, and X. Pan, Enhanced polarization and abnormal flexural deformation in bent freestanding perovskite oxides, Nat. Commun. **13**, 5116 (2022).

[11] L. Han, C. Addiego, S. Prokhorenko, M. Wang, H. Fu, Y. Nahas, X. Yan, S. Cai, T. Wei, Y. Fang *et al.*, High-density switchable skyrmion-like polar nanodomains integrated on silicon, Nature (London) **603**, 63 (2022).

[12] J.-K. Huang *et al.*, High-κ perovskite membranes as insulators for two-dimensional transistors, Nature (London) **605**, 262 (2022).

[13] N. A. Pertsev, V. G. Kukhar, H. Kohlstedt, and R. Waser, Phase diagrams and physical properties of single-domain epitaxial $Pb(Zr_{1-x}Ti_x)O_3$ thin films, Phys. Rev. B **67**, 054107 (2003).

[14] O. Diéguez, K. M. Rabe, and D. Vanderbilt, First-principles study of epitaxial strain in perovskites, Phys. Rev. B **72**, 144101 (2005).

[15] O. Diéguez, O. E. González-Vázquez, J. C. Wojdeł, and J. Íñiguez, First-principles predictions of low-energy phases of multiferroic $BiFeO_3$, Phys. Rev. B **83**, 094105 (2011).

[16] T. Angsten, L. W. Martin, and M. Asta, Orientation-dependent properties of epitaxially strained perovskite oxide thin films: Insights from first-principles calculations, Phys. Rev. B **95**, 174110 (2017).

[17] L. Zhang, J. Han, H. Wang, R. Car, and E. Weinan, Deep potential molecular dynamics: A scalable model with the accuracy of quantum mechanics, Phys. Rev. Lett. **120**, 143001 (2018).

[18] B. Jaffe, R. S. Roth, and S. Marzullo, Piezoelectric properties of lead zirconate-lead titanate solid-solution ceramics, J. Appl. Phys. **25**, 809 (1954).

[19] L. Han, X. Yang, Y. Lun, Y. Guan, F. Huang, S. Wang, J. Yang, C. Gu, Z.-B. Gu, L. Liu, Y. Wang, P. Wang, J. Hong, X. Pan, and Y. Nie, Tuning piezoelectricity via thermal annealing at a freestanding ferroelectric membrane, Nano Lett. **23**, 2808 (2023).

[20] H. Fu and R. E. Cohen, Polarization rotation mechanism for ultrahigh electromechanical response in single-crystal piezoelectrics, Nature (London) **403**, 281 (2000).

[21] Z. Kutnjak, J. Petzelt, and R. Blinc, The giant electromechanical response in ferroelectric relaxors as a critical phenomenon, Nature (London) **441**, 956 (2006).

[22] Y. M. Jin, Y. U. Wang, A. G. Khachaturyan, J. F. Li, and D. Viehland, Adaptive ferroelectric states in systems with low domain wall energy: Tetragonal microdomains, J. Appl. Phys. **94**, 3629 (2003).

[23] Y. M. Jin, Y. U. Wang, A. G. Khachaturyan, J. F. Li, and D. Viehland, Conformal miniaturization of domains with low domain-wall energy: Monoclinic ferroelectric states near the morphotropic phase boundaries, Phys. Rev. Lett. **91**, 197601 (2003).

[24] P. E. Blochl, Projector augmented-wave method, Phys. Rev. B **50**, 17953 (1994).

[25] G. Kresse and D. Joubert, From ultrasoft pseudopotentials to the projector augmented-wave method, Phys. Rev. B **59**, 1758 (1999).

[26] G. Kresse and J. Furthmüller, Efficient iterative schemes for *ab initio* total-energy calculations using a plane-wave basis set, Phys. Rev. B **54**, 11169 (1996).

[27] G. Kresse and J. Furthmüller, Efficiency of ab-initio total energy calculations for metals and semiconductors using a plane-wave basis set, Comput. Mater. Sci. **6**, 15 (1996).

[28] J. P. Perdew, A. Ruzsinszky, G. I. Csonka, O. A. Vydrov, G. E. Scuseria, L. A. Constantin, X. Zhou, and K. Burke, Restoring the density-gradient expansion for exchange in solids and surfaces, Phys. Rev. Lett. **100**, 136406 (2008).

[29] D. Vanderbilt and M. H. Cohen, Monoclinic and triclinic phases in higher-order devonshire theory, Phys. Rev. B **63**, 094108 (2001).

[30] M. Ahart, M. Somayazulu, R. E. Cohen, P. Ganesh, P. Dera, H. K. Mao, R. J. Hemley, P. Ren, Y. a nd Liermann, and Z. G. Wu, Origin of morphotropic phase boundaries in ferroelectrics, Nature (London) **451**, 545 (2008).

[31] R. Guo, L. E. Cross, S.-E. Park, B. Noheda, B. Noheda, D. E. Cox, and G. Shirane, Origin of the high piezo electric response in $PbZr_{1-x}Ti_xO_3$, Phys. Rev. Lett. **84**, 5423 (2000).

[32] B. Noheda, D. E. Cox, G. Shirane, J. A. Gonzalo, L. E. Cross, and S.-E. Park, A monoclinic ferroelectric phase in the $Pb(Zr_{1-x}Ti_x)O_3$ solid solution, Appl. Phys. Lett. **74**, 2059 (1999).

[33] J. Wu, J. Yang, L. Ma, L. Zhang, and S. Liu, Modular development of deep potential for complex solid solutions, Phys. Rev. B **107**, 144102 (2023).

[34] https://github.com/huiihao/Spiral, Available online.

[35] S. Plimpton, Fast parallel algorithms for short-range molecular dynamics, J. Comput. Phys. **117**, 1 (1995).

[36] See Supplemental Material at http://link.aps.org/supplemental/10.1103/PhysRevLett.133.046802, which includes Refs. [33,35,37,38], for additional discussions on computational methods, three-dimensional real-space dipole distributions, piezoelectric response, Landau-Ginzburg-Devonshire model, and superlattices for dipole spirals.

[37] R. He, H. Wu, L. Zhang, X. Wang, F. Fu, S. Liu, and Z. Zhong, Structural phase transitions in $SrTiO_3$ from deep potential molecular dynamics, Phys. Rev. B **105**, 064104 (2022).

[38] M. J. Haun, E. Furman, S. Jang, H. McKinstry, and L. Cross, Thermodynamic theory of $PbTiO_3$, J. Appl. Phys. **62**, 3331 (1987).

[39] Y. Tsunoda, Spin-density wave in cubic γ-Fe and γ-$Fe_{100-x}Co_x$ precipitates in Cu, J. Phys. Condens. Matter **1**, 10427 (1989).

[40] Y. Tsunoda, Y. Nishioka, and R. Nicklow, Spin fluctuations in small γ-Fe precipitates, J. Magn. Magn. Mater. **128**, 133 (1993).

[41] Y. L. Li, S. Y. Hu, Z. K. Liu, and L. Q. Chen, Phase-field model of domain structures in ferroelectric thin films, Appl. Phys. Lett. **78**, 3878 (2001).

[42] P. Kavle, J. A. Zorn, A. Dasgupta, B. Wang, M. Ramesh, L.-Q. Chen, and L. W. Martin, Strain-driven mixed phase domain architectures and topological transitions in $Pb_{1-x}Sr_xTiO_3$ thin films, Adv. Mater. **34** (2022).

[43] B. Noheda, D. E. Cox, G. Shirane, S.-E. Park, L. E. Cross, and Z. Zhong, Polarization rotation via a monoclinic phase in the piezoelectric 92% $PbZn_{1/3}Nb_{2/3}O_3$-8% $PbTiO_3$, Phys. Rev. Lett. **86**, 3891 (2001).

[44] T. Koo and S. Cheong, Dielectric and piezoelectric enhancement due to 90° domain rotation in the tetragonal phase of $Pb(Mg_{1/3}Nb_{2/3})O_3$-$PbTiO_3$, Appl. Phys. Lett. **80**, 4205 (2002).

[45] J. C. Wojdeł and J. Íñiguez, Ferroelectric transitions at ferroelectric domain walls found from first principles, Phys. Rev. Lett. **112**, 247603 (2014).

[46] D. D. Khalyavin, R. D. Johnson, F. Orlandi, P. G. Radaelli, P. Manuel, and A. A. Belik, Emergent helical texture of electric dipoles, Science **369**, 680 (2020).

[47] H. Zhu, J. Yi, M.-Y. Li, J. Xiao, L. Zhang, C.-W. Yang, R. A. Kaindl, L.-J. Li, Y. Wang, and X. Zhang, Observation of chiral phonons, Science **359**, 579 (2018).

[48] H. J. Zhao, P. Chen, S. Prosandeev, S. Artyukhin, and L. Bellaiche, Dzyaloshinskii-Moriya-like interaction in ferroelectrics and antiferroelectrics, Nat. Mater. **20**, 341 (2021).